Natural Hazards
https://doi.org/10.1007/s11069-025-07403-z

ORIGINAL PAPER

Local seismic response in the historical centre of Nafplio (Greece) as a tool for seismic risk management

Matteo Fiorucci[1,8] · Salvatore Martino[2] · Benedetta Antonielli[2] · Vasiliki (Betty) Charalampopoulou[3] · Paolo Ciampi[2] · Yawar Hussain[2] · Roberto Iannucci[4] · Daniele Inciocchi[2] · Vassilis Karastathis[5] · Charilaos Maniatakis[6] · Eirini Marinou[3] · Aggelos Mouzakiotis[5] · Stefano Rivellino[2] · Charalampos Saroglou[7] · Athina Tsirogianni[7] · Francesca Bozzano[2]

Received: 16 October 2024 / Accepted: 22 May 2025

Abstract
Analysis of local seismic response is a crucial tool for assessing site-specific seismic hazards, particularly in urban areas of cultural and historical significance. However, these analyses often overlook the complexities of near-surface geological and topographical conditions, especially in regions with medium to high seismic activity. This study, funded by the H2020RISE-Marie Curie Action in the framework of the STABLE (STructural stABiLity risk assEssment) project, focuses on the local seismic response of Nafplio (Greece), an urban area rich in cultural heritage. By adopting an integrated methodology, we aim to enhance the understanding of seismic risk in complex subsoil environments. The approach involves: (i) constructing a 3D geological model of the area's subsoil setting, including it in an engineering geological modelling; (ii) estimating the resonance frequency of the soft soils using ambient seismic noise measurements and earthquake-based geophysical techniques; (iii) generating response spectra for three return periods of 50, 475, and 2000 years using both 1D and 2D numerical modelling approaches. A strict integration of engineering geological, geophysical and numerical modelling results provided a more robust framework for evaluating local seismic amplification in a geologically complex urban contest, where both stratigraphic and topographic effects can be expected to act in modifying the seismic shaking scenario, so offering a valuable example of a work frame adapt to manage risk mitigation in a increasing resilience perspective for high seismicity urban areas.

Keywords Local seismic response · Engineering geological model · Geophysical investigations · Seismic numerical modelling · 3D geological reconstruction

1 Introduction

The severity of earthquake damage scenarios in urban areas is typically a result of a combination of local seismic amplification effects (Sextos et al. 2018) and the inherent seismic vulnerability of the built environment (Sorrentino et al. 2019). Local seismic

Extended author information available on the last page of the article

response analysis plays a key role in understanding and mitigating these hazards, particularly in the context of seismic microzonation approaches. The accuracy of the local seismic response analysis largely depends on the reliability of the engineering geological model, as it represents the reference for conceptualising seismic responses and designing numerical simulations, as well as on the properties of the materials involved, including both soils and rocks. In addition to stratigraphic amplification, complex geological conditions of the subsoil can obscure or influence the interpretation of local seismic response, with effects arising from processes that differ from stratigraphic amplification alone (Martino et al. 2020).

Over the past few decades, there has been increasing recognition in the literature of the need for an integrated approach to seismic hazard assessment. Such approaches combine engineering geological modelling, geophysical investigations, and numerical simulations to evaluate seismic shaking at specific sites (ICMS Working Group 2008; Gaudiosi et al. 2014; Martino et al. 2015; Macerola et al. 2019; Moscatelli et al. 2020; Pergalani et al. 2020; Varone et al. 2021; Aydin et al. 2025). These approaches are particularly relevant for evaluating seismic risks in areas with complex geological conditions (Kham et al. 2013; Salameh et al. 2017; Semblat et al. 2000; Hakimov et al. 2021, 2024).

The accuracy of local seismic response analysis is closely tied to the reliability of the engineering geological subsoil reconstruction, which allows the conceptualisation of seismic behaviour and the design of numerical models. Several studies have been published so far where 2D numerical approaches have been proved to be a valuable tool in local seismic response analysis. By simulating the propagation of seismic waves from the seismic bedrock to the surface, these models account for the lateral and vertical variations of the physical and mechanical properties of soils as well as their stratigraphy, including lateral heterogeneities and complex topographical features (Martino et al. 2015; Sonmezer et al. 2019; Tunar Özcan et al. 2019; Antonielli et al. 2021; Moscatelli et al. 2021; Tallini et al. 2020).

Dealing with the cultural heritage protection topic, the H2020—RISE "STABLE—Structural stABLity risk assEsment" project (www.stable-project.eu; Serpetti et al. 2020) aims at assessing both seismic action, through site-specific local seismic analysis, and the vulnerability of historic buildings to evaluate the damage scenario expected for the following historical centres of the Mediterranean area: Rieti (Italy) (Antonielli et al. 2023), Nafplio (Greece) (Saroglou et al. 2021) and Strovolos (Cyprus) (Iannucci et al. 2022).

This study focuses on assessing the local seismic response of Nafplio town (Greece), an important cultural and tourist hub located in the Argolic Gulf in northeastern Peloponnese, Greece (Fig. 1). The town's complex geological setting, characterised by two steep-slope reliefs (called Acronafplia and Palamidi) and by a coastal plain, presents a good opportunity for seismic hazard analysis involving an historical town located in an area affected by medium to high seismic hazards. Because of the complex geological conditions, a high-resolution 3D geological model was developed to produce detailed zonation for the area in terms of seismic response, a significant advancement in the field. Recent advances in modelling technologies have enabled the reconstruction of subsurface structures through simple cross-sections and by creating 3D models which envelope the volumes of interest. These large-scale models have already been applied in local seismic response studies (Bala et al. 2023; Giallini et al. 2024).

The local seismic response analysis of the Nafplio historical town includes several key steps: (i) assessment of the basic seismic hazard for different return periods, (ii) reconstruction of an engineering geological model of the subsoil, (iii) execution of single-station seismic ambient noise measurements, (iv) 2D numerical simulations, (v) standard spectral ratio (SSR) analysis using recorded earthquakes data; (vi) seismic microzonation mapping.

The results aim to provide a comprehensive understanding of seismic risk in the historical town of Nafplio and offer valuable insights for risk mitigation and resilience strategies in seismic-prone areas with cultural heritage significance.

2 Geological and geomorphological settings

The Nafplio town is in the Argolis Peninsula, which is part of the more extended Dinaric-Hellenic orogenic system (Fig. 1), including a complex thrust-belt frame of tectonic flaps with a NW–SE trend and with northwest vergence, generated during the Alpine-Himalayan orogenesis by the collision between the Adria plate and the south sector of the Eurasia Macroplate (Auboin 1959, 1970; Bortolotti et al. 2013), which widely involves sedimentary and metamorphic units. The Hellenides surround the southern part of the mountain chain and the area of Nafplio consists of a succession of 5 tectonic units, which in sequence, from bottom to top, are: (i) *Trapezona* unit (middle/lower Triassic—Upper Jurassic); (ii) ophiolitic unit of *Dhimaina* (middle Triassic—upper Jurassic / lower Cretaceous), composed of the ophiolitic complex of *Migdalista* and the mesoautoctonous series of *Lygourio*; (iii) *Iliokastron* melangitic unit (middle/upper Jurassic—lower Cretaceous, outcrop in northern Argolis); (iv) *Adheres* melangitic unit (Cretaceous—Paleocene, crop out in Southern Argolis); (v) *Faniskos* unit (upper Jurassic—Eocene). These 5 units were involved in compressive deformation with folding and northwest thrusting, resulting also in an inverted stratigraphic sequence.

The urban area of Nafplio was involved in a compressive tectonic phase during the Upper Jurassic, which brought the *Migdalista* ophiolitic complex above the Triassic-Jurassic limestones, these latter belonging to the *Trapezona* Unit.

During the middle Cretaceous, the Hellenid accretionary prism experienced intensive erosive episodes in the subaerial environment, with coarse clastic breccias rich in basalts and limestone deposition, while in the Upper Cretaceous and in the Paleocene, pelagic limestones overlapped by siliciclastic flysch were sedimented (Photiades 2010) in a geological sequence which is named meso-autochthonous series of *Lygourio,* following Bortolotti et al. (2003).

A further compressive tectonic phase occurred during the late Eocene, according to Photiades (2010), which resulted in the simultaneous overthrust of the *Adheres* unit and the *Faniskos* unit above the flysch.

The geological formations outcropping in the Nafplio town (Apostolidis and Koutsouveli 2010) area include (from the oldest to the most recent, using the codes presented in the geological map of Fig. 2):

- Limestone (Lower Cretaceous—Upper Cretaceous; coded: Ki-s.k): white to grey massive limestone with medium-thick layers and good geomechanical characteristics;
- Limestone with chert (Campaniano—Maastrichtiano; coded: Ks.k2): white thin layers of limestone with cherts;
- Limestone with chert (Upper Cretaceous—Paleocene, coded: Ks.k1): white or pink to reddish thinly stratified limestone with chert; good geomechanical characteristics;
- Flysch (post-Ypresiano, coded: fg1): alternations of sandy marls, quartzite sandstones, siltstones and conglomerates with limestone;

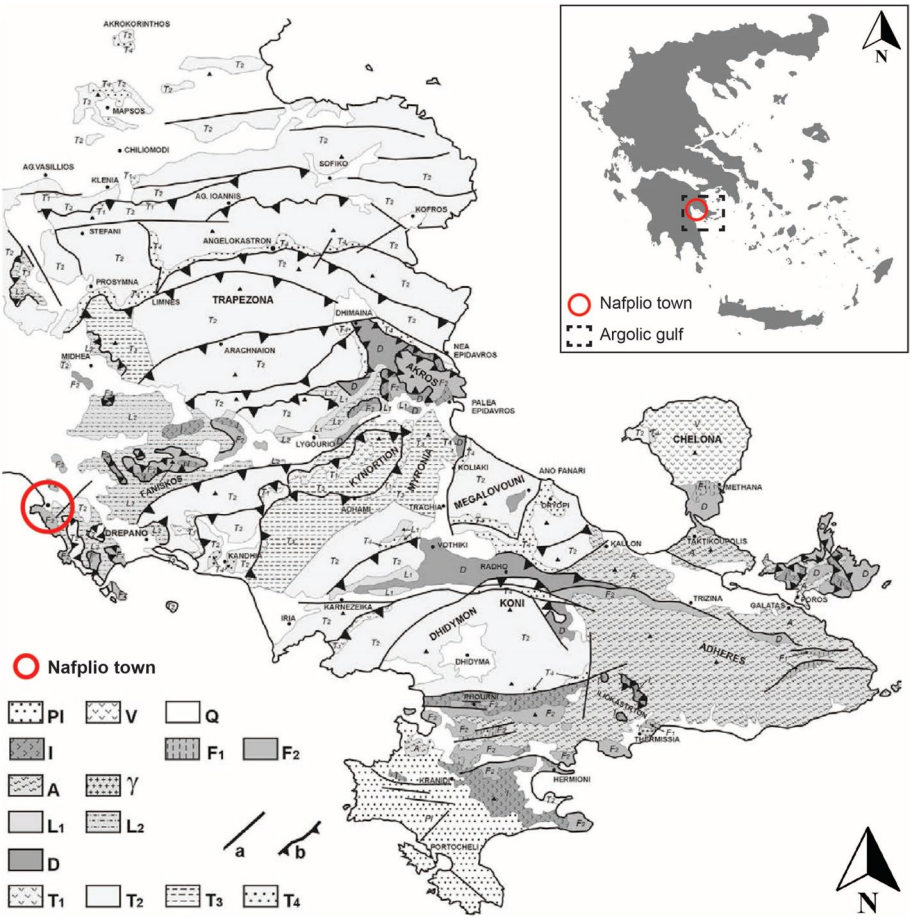

Fig. 1 Structural and stratigraphic map of the Argolic peninsula modified after Bortolotti et al. (2003). The legend codes are explained in the following: T1, T2, T3, T4: Layers belonging to the Trapezona Unit including (Lower Triassic—Lower Jurassic); (D) Dhimaina Ophiolitic Unit: (Lower Triassic—Lower Cretaceus); (L1, L2) Layers belonging to the Lighourio Meso-Autochthonous Unit— (Upper Albian-Cenomanian –post-Lower Eocene); (A) Adheres Mélange Unit,including (and overlain by) tectonic slices of Middle-Upper Jurassic granodiorite megablocks (γ); (I) Iliokastron Mélange Unit (middle/upper Jurassic—lower Cretaceous). heared serpentinites, strictly associated with various blocks of volcanics, serpentinised harzburgites, dunites, boninitic rocksand metamorphites; (F1, F2) Layers belonging to the Faniskos Unit—(Kimmeridgian- Palaeocene); (PI) Marine deposits (Upper Miocene—Lower Pliocene). (V) lavas and pyroclastic deposits (Lower Pleistocene—Holocene). (Q) Quaternary deposits. (a) faults. (b) thrust

- Conglomerates (Upper Pleistocene, coded: Pt.st.): pebbles of fossiliferous limestone of different origins and a red clayey cement. Comparable to soft rock with sufficient geomechanical characteristics;
- Gravels and breccias (Pleistocene, coded: Pt.sc1): from cohesive to semi-cohesive coarse clasts (mainly calcareous) and reddish cement. Comparable to soft rock with poor geomechanical characteristics;
- Gravel (Quaternary—Holocene, coded: Q.sc): pebbles and limestone fragments in a sandy-clayey matrix;

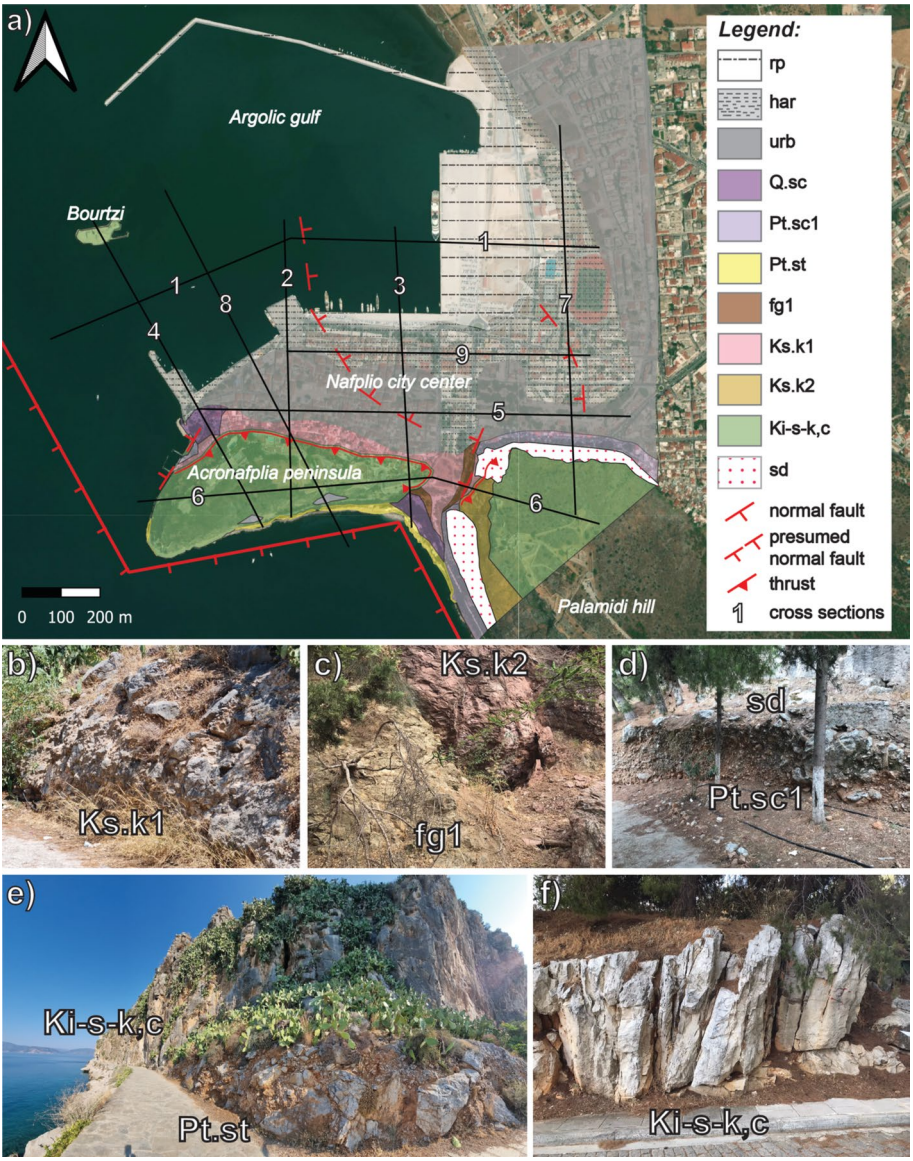

Fig. 2 Geological map of the Nafplio study area (**a**). The acronyms on the legend are explained in the following: rp—man-made ground post-1960; har and urb—man-made ground pre-1960; Q.sc—Screes (Holocene); Pt.sc1—Screes and breccias (Pleistocene) (box d); Pt.st—Conglomerate (Upper Pleistocene) (box e); Ks.k2—Limestones with cherts (Campanian–Maastrichtian) (box c); Ki-s.k,c—Limestones (Lower–Upper Cretaceous) (boxes e and f); fg1—Flysch (Post-Ypresian) (box c); Ks.k1—Limestones with cherts (Upper Cretaceous-Paleocene) (box b); sd—slope debris (box d)

- Filling materials (Holocene) which can be divided into: (i) recent loose deposits and man-made fill (coded: har), consisting of sandy clays, sands and gravels; variable thickness from 1 to 3.5 m (in some points, it exceeds 4 m); (ii) historical and younger depos-

its (coded: urb), consisting of construction materials and sandy-clayey soils; thicknesses less than 1 m.

The above-mentioned formations are represented in a revised geological map of the Nafplio study area, starting from the 1:5000 scale geological map of the Nafplio region (Fotiadis and Mitropoulos 2006), the information contained in Georgiou and Galanakis (2010), and the engineering geological surveys carried out on-site in 2020 and 2021 summer seasons.

The study area is characterised by the mountainous landscape prevailing in the south and the flat landscape dominating to the north. The prominent topographic features are Palamidi ridge on the southeast (223 m), the Acronafplia ridge (85 m) on the south and Bourtzi Island 600 m northwest of the harbour. The steep slopes of these ridges formed following the combination of both the horst and graben tectonics and the glacio-eustatic fluctuations of the sea level, which caused the abrasion and retreat of the sea cliffs, as well as the formation of marine terraces, and the deposition of the marine and continental conglomerates along the southern slope of the Acronafplia ridge (Georgiou and Galanakis 2010). Here, the sheet waters caused a wide cover erosion on the slopes with a consequent accumulation of colluvium at the slope bottom.

The geomorphological evolution of the Nafplio area was deduced by analysing landforms and sequences of morpho-evolutionary episodes were reconstructed. The tectonics generated a horst and graben tectonic setting, which influenced the river network and subsequent marine sedimentation (Mitropoulos and Zananiri 2010). The tectonic phases also contributed to shaping the steep slopes which characterise the southern and north-western sides of the Acronafplia peninsula, as well as of the Palamidi ridge. The sea level glacio-eustatic fluctuations also produced the coastal erosion and retreat of the sea cliffs, which characterise the southern and north-western sectors of the Acronafplia ridge. Moreover, climatic marine terraces overlapped by marine conglomerates outcrop along the Arvanitia trail, south of the Acronafplia ridge (Georgiou and Galanakis 2010).

3 Seismic hazard/earthquake scenario

Seismic hazard analysis represents a widely applied tool for estimating the strong motion amplitude at a specific return time; therefore, such an analysis provides a fundamental input in earthquake risk mitigation planning (McGuire 1993).

Seismic hazard is a quantitative estimation of ground shaking, defined by morphometric analysis. It includes peak ground acceleration (PGA), velocity (PGV), displacement (PGD), or response spectrum ordinates. Therefore, seismic hazard analysis involves the estimation of the most crucial parameters related to seismic hazard that is expected to occur at a given site during a predefined time interval (the return period—probabilistic approach, PSHA) or for specific earthquake scenarios (deterministic approach, DSHA). In the present study, both the probabilistic and the deterministic approaches are used for the seismic hazard assessment of the Nafplio Historical Centre. In particular, the PSHA methodology was first carried out to calculate the level of ground shaking for specific return periods. Using the calculated PGA values as a basis, we then used the DSHA methodology to obtain synthetic time series for earthquake scenarios from the local active faults, aiming to obtain these PGA values.

3.1 Seismotectonic and seismicity

The study area is located on the Hellenic subduction zone, which is characterised by the subduction of the African plate under the overriding Aegean plate. The subduction of the African plate is located several tens of kilometres under the broader area of Nafplio and thus, mostly intermediate to deep events occur in the region directly surrounding the town. According to the earthquake catalogue of Papazachos and Papazachou (2003), several strong events have occurred in the broader Eastern Peloponnese region, with magnitudes up to M 7.0 (Fig. 3). The actual depth of these historical events cannot be determined accurately, however, by examining the recently recorded seismicity (Fig. 3), it can be deduced that those occurred in the close vicinity of Nafplio are probably of intermediate to large depth, related to the subduction zone. Shallow fault zones have been documented, however, to the east and north of the study area (Fig. 3), which can be attributed to some past strong events such as:

- The Iria fault zone (Papazachos and Papazachou 2003; Karakaisis et al. 2010), a North dipping normal fault possibly related to several historical events with M > 6.0, with the most notable being the M6.4 earthquake of 1769, which caused significant damage to the town of Nafplio;
- The Epidaurus fault zone (Karakaisis et al. 2010), which can be related to an M6.3 event that occurred in 1837;

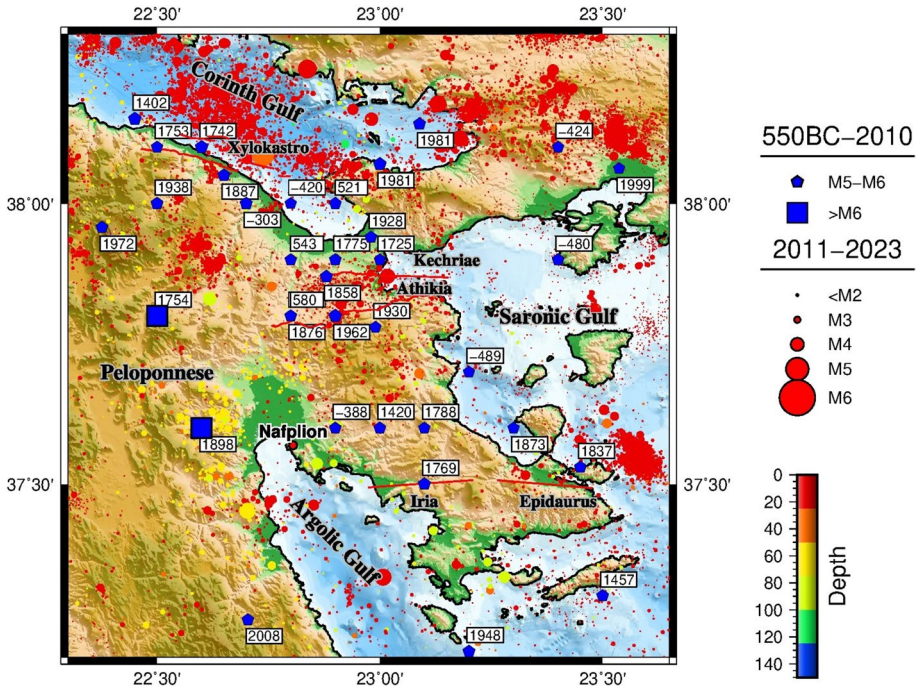

Fig. 3 Map showing the major historical earthquakes and main faults in the broader region of NE Peloponnese (Papazachos and Papazachou 2003), along with the recorded seismicity for the period between 1/2011 and 6/2022 (source: National Observatory of Athens)

- The Athikia fault zone (Karakaisis et al. 2010), a series of north-dipping normal faults, related to an M6.5 event in 1858;
- The Kechriae fault zone (Noller et al. 1997), also a north-dipping normal fault related to several M > 6.0 events in the area around Corinth;
- The Xylokastro fault zone (Ferentinos et al. 1988; Armijo et al. 1996) located in the southeastern part of the Gulf of Corinth, attributed to the large M6.7 earthquake of 1742.

3.2 Basic seismic hazard assessment

The basic seismic hazard assessment for the area of interest was performed in probabilistic and deterministic contexts. The probabilistic seismic hazard assessment (PSHA) was carried out on the basis of the following steps (Reiter 1990; Baker 2008): (i) identification of all regional active sources, (ii) determination of the local seismicity parameters for the seismic sources (magnitude of completeness (Mc), b-value, seismicity rate), (iii) establishing a source distance distribution model, which refers to the distribution of the sources within the study region, relative to the Nafplio town, (iv) calculating the distribution of ground motion on the basis of the Ground Motion Prediction Equation (GMPE) and v) final calculation of the seismic hazard by combining the above-mentioned elements. Regarding the input sources in our case, we followed a fault-based approach, using the active sources described previously. The calculation of the local seismicity parameters is directly linked to the completeness of the implemented earthquake catalogue. In fact, a homogeneous catalogue should be implemented to reliably estimate the seismicity rate in any given region. The estimation of those parameters was based on the earthquake catalogue of Papazachos and Papazachou (2003) for the historical events, combined with the updated earthquake catalogue of Makropoulos et al. (2012) and the recently recorded seismicity by the National Observatory of Athens (NOA). The combined catalogue that resulted spans a period between 1968 up to 2020. The actual magnitude of completeness for the implemented catalogue was evaluated at M2.6, using the Maximum Curvature method proposed by Wiemer and Wyss (2000). This value is mostly related to the completeness of the early instrumental period that is covered by this catalogue. The parameters related to the seismicity rate were calculated based on the Modified Gutenberg-Richter law (Cornell and Vanmarke 1969; Sornette and Sornette 1999), whereas the selection of the maximum magnitude was based on the scaling laws of Wells and Coppersmith (1994), for each of the individual active sources. The GMPE proposed by Danciu and Tselentis (2007) for the Greek region was applied and as the last step, the PGA distribution for different return periods was obtained by applying the total probability theorem. Similarly, the Pseudo Spectral Acceleration (PSA) was also calculated for the spectral periods specified in the above GMPE. The resulting hazard curves and PSA spectra for return periods of 475, 950 and 2000 years for the town of Nafplio can be seen in Fig. 4. The corresponding calculated PGA values for the three return periods are 65, 85 and 120 cm/s^2, respectively.

For the Deterministic Seismic Hazard Assessment (DSHA), we used the previously described seismic sources and simulated several seismic scenarios for them, to obtain synthetic acceleration waveforms with PGA values like those obtained by the PSHA technique, as well as for the worst-case earthquake scenario (maximum possible magnitude for each fault, based on the scaling law of Wells and Coppersmith 1994). Our purpose was to obtain accelerograms that were characteristic of the local faults and, at the same time, took into consideration the seismic hazard that was calculated for different return

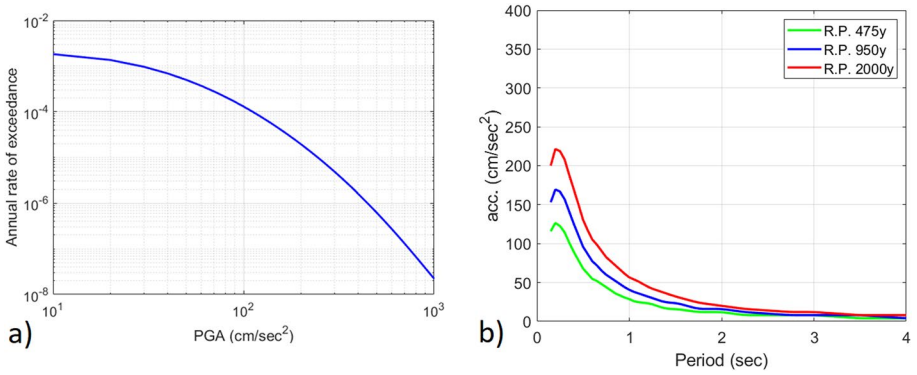

Fig. 4 **a** Hazard curve for the site of Nafplio reported as Peak Ground Acceleration (PGA) vs. annual rate of exceedance, **b** Pseudospectral acceleration (PSA) with 475, 950 and 2000 years return periods for the town of Nafplio

periods, according to the PSHA methodology. The simulation methodology that was used was the stochastic simulation of ground motion (Boore 1983) expanded for finite sources by Beresnev and Atkinson (1997). More specifically, we employed the EXSIM algorithm (Motazedian and Atkinson 2005), which implements a dynamic corner frequency, further improving the results (Table 1). According to the stochastic simulation methodology, the acceleration time series A(t) that is observed in a specific site is the result of the convolution of the source S(t), the path P(t) and the local site effect G(t). Each individual source was implemented as a planar surface, subdivided into a series of point sub-sources, distributed relative to the location and the geometrical characteristics of the fault (length, width, strike, dip). The final synthetic time series is obtained by convolving the individual calculated time series for each point sub-source.

Since the aim of the application of the above methodology was the calculation of synthetic accelerograms with specific PGA values, the simulations were carried out for a range of magnitudes and stress drop values for each fault. Consequently, the fault dimensions

Table 1 Main parameters used with the EXSIM algorithm for the calculation of the various synthetic accelerograms

Stress drop		30–80
Hypo loc		Random
Dt (sampling step)		0.002 s
Vs (shear wave velocity)		3.4 km/s
Rho (density)		2.8 kg/m^3
Vrup (rupture velocity)		0.8VS
Geometrical spread		1/R
Q model (Inelastic attenuation model)	Q0	55
	n	0.91
window		
Pulsing percentage		50
Slip distribution		random
K0 (Seismic spectrum amplification factor at high frequencies)		0.035

varied, depending on the earthquake magnitude that was simulated. The VS velocity and density at the depth of each fault were set at 3.4 km/s and 2.8 kg/m^3 respectively, which are common values for depths between 5 and 15 km for Greek continental crust in the broader region. The rupture velocity was set at 80% of the VS. Regarding the path effect, a 1/R geometrical spreading model related to propagation in homogeneous space was used since the source-to-site distances for all scenarios are relatively small (< 80 km), and thus, crustal heterogeneity is not expected to play any major role. The anelastic attenuation model that was used was the one proposed by Polatidis et al. (2003), which was based on real recordings of back-arc events in the Greek region and finally, the duration model of Atkinson and Boore (1995) was also implemented. The site effect is represented by an amplification versus frequency curve. In our case, we used the attenuation coefficients proposed by Klimis et al. (1999) for soil class A (rock) in combination with the proposed value of 0.035 for the K_0 value by the same authors. The final synthetic time series were calculated after several iterations for random hypocentre locations and slip distributions.

Based on the obtained synthetic acceleration time series, a set of 7 recordings of real earthquakes was selected for each return period (i.e., 50, 475, and 2000 years) using the REXELweb tool (Sgobba et al. 2021) by the National Institute of Geophysics and Volcanology INGV (http://itaca.mi.ingv.it/ItacaNet_31/#/data_and_services/tools/rexel). The selection was performed using the mean elastic response spectrum computed on the synthetic accelerograms for each return period as a target for the tool, therefore ensuring the spectro-similarity between the target response spectrum and the mean elastic response spectrum of the 7-time histories selected for each return period from the Engineering Strong Motion Database (ESM) and the Italian Accelerometric Archive (ITACA). The selected time histories were used in the subsequent steps of this work to perform seismic wave propagation simulations aimed at calibrating the subsoil models as well as assessing the expected seismic shaking of the site.

4 Local seismic response analysis

The conceptual workflow (Fig. 5) that leads to the evaluation of the expected seismic action at Nafplio town started with the construction of the preliminary geological model based on existing literature and the stratigraphy of the previously available surveys. The interpreted

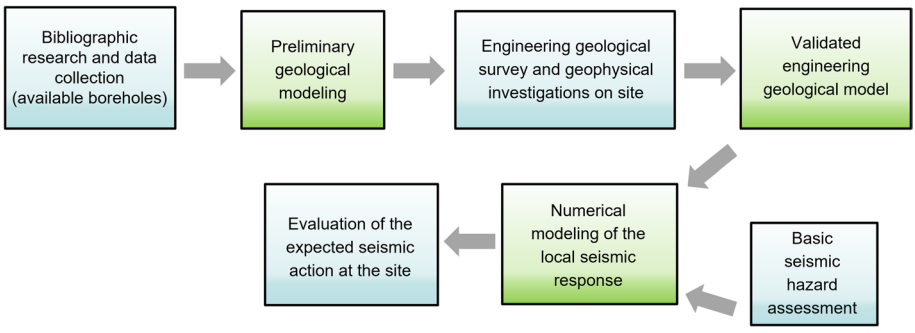

Fig. 5 Proposed workflow for the local seismic response analysis carried out for this study in a framework of the STABLE project

geological cross-sections of the historical town centre represented the geological model of reference that has been validated using a large set of in-situ geophysical survey results, i.e., by fitting site resonance frequency (f_0) with the main peak of the amplification function obtained by the 1D linear elastic modelling of the corresponding site stratigraphy.

The validated engineering geological model has been represented in a 3D model, which allows observing the spatial relationships between different geological bodies with marked differences in physical and mechanical properties. The reliability of local seismic response analyses is indeed directly related to the accuracy of the engineering geological reconstruction of the near-surface subsoil.

A 2D numerical modelling of seismic motion has been performed with an equivalent linear approach (finite elements) with LSR 2D (by the software STACEC, stacec.com, licensed to Sapienza) on 4 selected engineering geological cross-sections to extract the time histories and elastic response spectra (5% damping) from 124 control nodes distributed all along the cross sections.

4.1 Engineering-geological modelling

The reconstruction of an engineering geological model of the Nafplio area has been achieved using several previous investigations and the data collected from the on-site geological and engineering geological surveying, as well as previous scientific literature (Karastathis et al. 2010).

Regarding the previously available data, the following dataset has been accounted for:

- Geophysical investigations: data of a seismic reflection campaign conducted by the Hellenic Survey of Geology & Mineral Exploration (HSGME) with the morphological and stratigraphic reconstruction of the seabed of the Gulf of Nafplio, thanks also a bathymetric map at a scale of 1:5000. Through the seismic reflection, the geological structures below the seabed were also outlined with the identification of 3 unconformities, which define four seismic units. HSGME also conducted, both in the coastal area and the hinterland of Nafplio, a series of seismic reflection surveys to detect the depth of the bedrock and the possible presence of faults. HSGME also carried out 4 cross-hole investigations, 2 of which are close to the town of Nafplio. Results show the presence of a loose deposit, consisting of clay and silt, with S-wave velocities of less than 400 m/s. The velocity of the P-waves is instead higher than 1500 m/s, probably also due to the saturation of the deposit because of the sea water entry;
- Boreholes: a total of 21 boreholes, 17 offshore, in the port area, and 4 on land (performed by Triton Consulting Engineers S.A., Geomichaniki, HSGME) have been consulted. The same stratigraphic sequence characterised the analysed boreholes, with differences in the thickness of the lithotypes: off the harbour to the northwest, between the coast and Bourtzi island, the terrigenous component is prevalent, while in the northern sector of the offshore of the ancient town, the terrigenous component is lower than the lithoid one. All the logs obtained from the boreholes were used to better constrain the preliminary geological model.

Together with the information derived from previous studies and the technical reports used to reconstruct the geological model of the plain and the gulf in front of Nafplio, two detailed geological and geotechnical field surveys were carried out in July 2020 and July 2021, mainly focused on the reconstruction of the geological model of the Acronafplia and

Palamidi reliefs and distribution of the recent deposits. The on-site survey at Acronafplia revealed that the hill is composed of heavily fractured Cretaceous limestone, with flysch outcropping in the depression towards Palamidi ridge. The survey along the ridge's southern and western sides confirmed susceptibility to rock falls and coastal erosion, leading to shoreline retreat. The N/NW side of Palamidi features a thrust with an NW vergence, where an inverted stratigraphic succession crops out. The thrust zone shows complex deformation, with fractured limestone, flysch, and striated calcite surfaces. The area between the ridges exhibits repeated outcrops, and a normal fault has lowered the Acronafplia peninsula. The northern slope of Palamidi is surrounded by a Pleistocene gravel deposit, which is in erosive contact with Eocene flysch and extends to the coast along the W-SW slope.

The available technical reports as well as the data collected during the two field surveys, allowed the definition of a detailed and updated geological map (Fig. 2). Furthermore, 9 geological cross-sections were obtained to better constrain the geological model of the subsoil (Saroglou et al. 2021), pointing out the geometries of the geological bodies and their lateral contacts (Fig. 6). A geotechnical map was then derived (Fig. 7) where the main lithotechnical units have been mapped.

4.2 Single-station seismic ambient noise measurements

A total of 99 single-station seismic ambient noise measurements were carried out to validate the geological model between 2020 and 2021, covering the urban area of Nafplio. The single-station seismic ambient noise measurements were performed using two different kinds of sensors: (i) LE-3D/5 s three-component seismometers (0.2 Hz eigenfrequency) together with REFTEK 130–01 dataloggers; (ii) SL06 24-bit digitisers with built-in SS20 three-component velocimeter (2.0 Hz eigenfrequency) by SARA Electronic Instruments. Seismic ambient noise was recorded for 1 h at each measurement site at a sampling

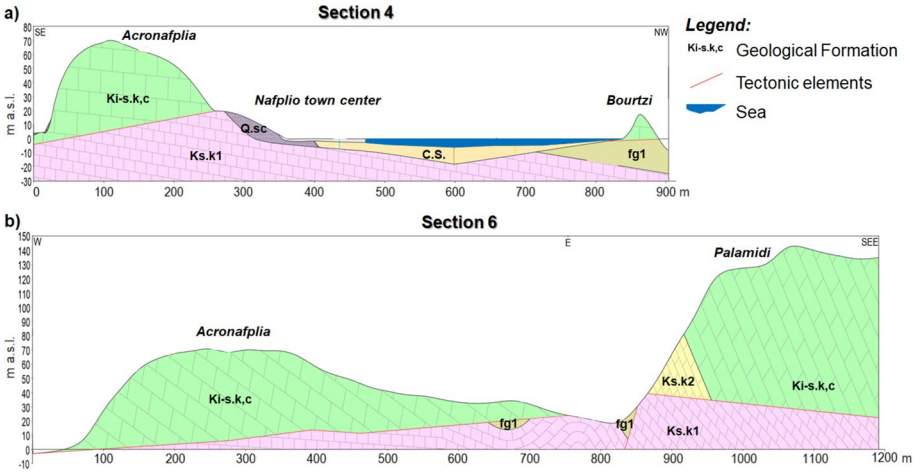

Fig. 6 Geological cross-sections n° 4 and n° 6 of the study area (for the location see Fig. 2) on which the geological formation codes are reported: C.S.—clayey sands and sandy clays (Quaternary)—Q.sc—Screes (Holocene); Ks.k2—Limestones with cherts (Campanian–Maastrichtian); Ki-s.k,c—Limestones (Lower–Upper Cretaceous); fg1—Flysch (Post-Ypresian); Ks.k1—Limestones with cherts (Upper Cretaceous-Paleocene)

Fig. 7 **a** Engineering geological map of the Nafplio study area. The orange diamonds mark the locations of the single-station seismic ambient noise measurement (HVNR) sites, along with the resonance frequency values (diamonds with no value means "no resonant site"), while the blue diamonds show the position of the earthquake recording stations (HVER) (*modified after* Antonielli et al. 2022). **b** Example of the equipment used for the single station for HVNR measurements. **c** Panoramic view of the study area; the locations of the earthquake recording stations (SS*n*) are also shown. The viewpoint of the panoramic picture is reported on the engineering geological map (eye-shaped icon)

frequency of 250 Hz. and elaborated by GEOPSY (Wathelet et al. 2020) with the following processing parameters:

- a 40 s windows with overlaps of 25% for each time serie;
- tapering to 5% and smoothing of the spectrum for each window by the algorithm of Konno and Omachi (1998) with the b parameter equal to 40;
- 0.2–20 Hz frequency range of the analysis.

The horizontal-to-vertical noise spectral ratio (HVNR) method, here utilised to elaborate the seismic ambient noise measurements, is commonly employed to assess the 1D stratigraphic resonance of locations where there is a significant contrast between the low S-wave velocity subsoil and the seismic bedrock beneath it (Haghshenas et al. 2008). In HVNR processing, the Fourier transforms (FFTs) of the horizontal ground motion components are averaged and subsequently divided by the FFT of the vertical component. Additionally, the software GEOPSY was employed to analyse the polarisation of the HVNR peak. The average HVNR function was computed in 10° increments from 0° to 180° and reconstructed on the horizontal plane as a function of azimuth.

The HVNR functions, obtained from the measurements carried out on the recent deposits of the Nafplio coastal plain, are characterised by a marked peak having frequency values of 2–5 Hz in the historical town centre (Fig. 8, left panel) and 1–2 Hz in the modern town area (Fig. 8, middle panel). No polarisation can be observed based on the Horizontal to Vertical Instantaneous Polarisation (HVIP) analysis performed by the software GEOPSY (Fig. 8, lowest row). These results can be related to the stratigraphic resonance of the

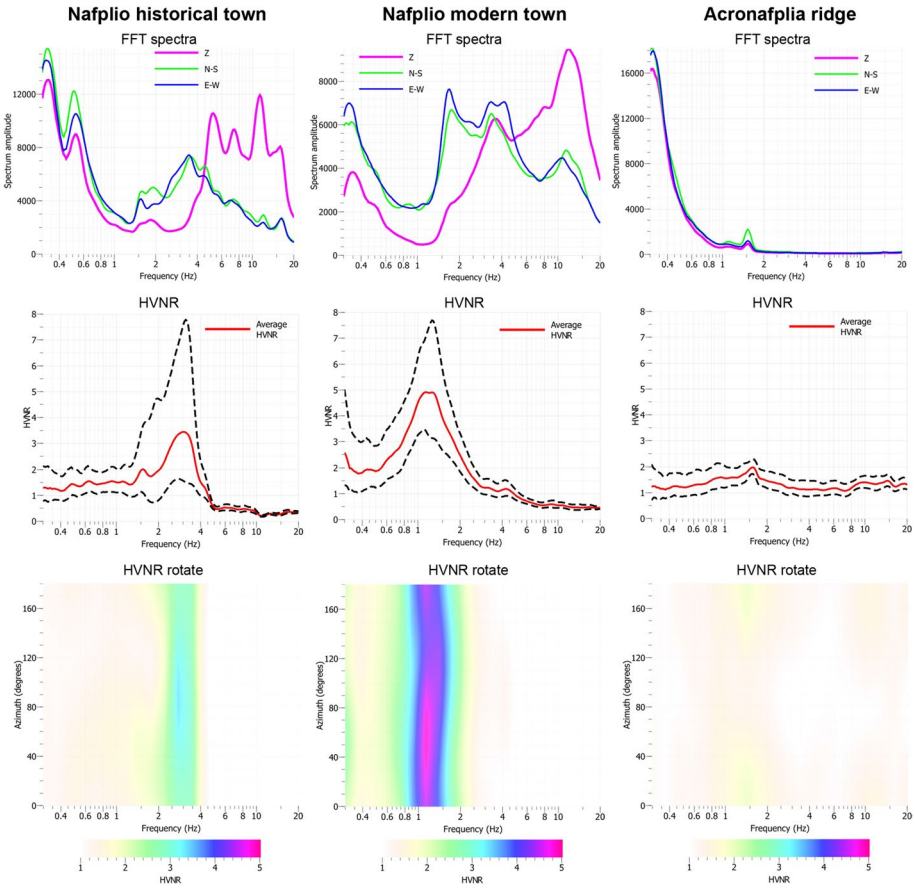

Fig. 8 Examples of FFT spectra, HVNR functions (the dashed black lines are the upper and lower limits of standard deviations) and HVNR rotate plot obtained at Nafplio historical town centre (left panel), Nafplio modern town (middle panel) and Acronafplia ridge (right panel) (*modified after* Saroglou et al. 2021)

coastal plain deposits, according to a depth-controlled seismic response model (Castellaro and Mulargia 2009; Martino 2024). In addition, the increase of the frequency resonance found from the measurements performed on the coastal plain (Fig. 7) can be referred to a decrease in the deposit thickness moving from the modern town to the historical centre area, always in agreement with a depth-controlled seismic response in model (Fig. 6). On the other hand, the HVNR functions, obtained from the seismic ambient noise measurements performed on the Acronafplia relief, do not show any significant peak (Fig. 8, right panel), according to a "stable" seismic response model (Martino 2024).

4.3 Engineering geological model validation

A preliminary modelling of seismic wave propagation was performed under elastic conditions to validate and calibrate the reconstructed engineering geological model. An iterative procedure (Moscatelli et al. 2021; Iannucci et al. 2022) based on the comparison between the amplification functions obtained by 1D numerical simulations of seismic wave propagation performed with the open-source software STRATA (Kottke and Rathje 2008), and the HVNR derived functions, obtained from the single-station seismic ambient noise measurements, were used as explained in the following.

A seismostratigraphy was derived from the engineering geological cross-sections of Nafplio in correspondence with the sites where the measurements were performed. Each seismostratigraphy contains a log of lithotechnical units (subsoil column) composed of a soft soil multilayer, with relative thickness supposed in the site, a seismic bedrock infinite half-space placed at a validated depth and a value, or a range of values associated with each unit based on geotechnical data already available. The numerical simulations were performed for each soil column by a linear elastic approach, varying firstly the values of unit weight volume (γ_n) and shear wave velocity (Vs) within the ranges defined for each lithotechnical unit and secondly the thickness of the lithotechnical units up to obtain a correspondence between the amplification function (i.e., the ratio of the FFT amplitude spectra at the subsoil surface and at the outcropping seismic bedrock) obtained by the numerical modelling and the HVNR peak from the seismic ambient noise measurements. Finally, the cross-sections were modified according to the thickness of the lithotechnical units obtained by the validation and calibration process.

Table 2 reports the physical and geotechnical parameters of each lithotechnical unit obtained by the validation and calibration procedure, which were used in the subsequent 2D numerical modelling to assess the expected seismic shaking. Based on available literature data, dynamic parameters of the soils, such as decay curves for damping and shear stiffness modulus, were attributed to the multilayer.

4.4 3D engineering geological modelling

Once validated, the engineering geological model has been exploited for the extrapolation of virtual stratigraphic boreholes at 358 points located along the 9 cross-sections previously validated. The spacing of the virtual boreholes, set equal to 50 m, locally descends to 10 m to increase the resolutive accuracy at complex geological structures. The geophysical-stratigraphic data collection belonging to a total of 406 points was stored in a geodatabase and processed using Rockworks 17 (Rockware Inc., licensed to Sapienza) for the generation of a 3D solid model (Song et al. 2019). The relational geodatabase constitutes a digital record collection model of georeferenced data that is stored in multiple Excel

Table 2 Parameters of the lithotechnical units obtained by the validating and calibrating process and used for the subsequent 2D numerical modelling

Litothecnical unit	γ_n (kN/m^3)	Vs (m/s)	Decay curve
Man-made fill	18	150	Elastic linear D = 2%
Clayey sands	20	170–240	Anastasiadis et al. (2001)
Marly-clayey flysch	19	300	National Seismic Service of Italy (2003)
Loose gravels	19	250	Lo Presti et al. (2002)
Sandy gravel	20	420	Lo Presti et al. (2002)
Conglomerates	23	750	Elastic linear D = 2%
Bedrock (limestones)	23	1100	Elastic linear D = 0.5%

In the legend: γ_n—unit weight of the soil in natural conditions, Vs—shear wave velocity

worksheets (Ciampi et al. 2021). Stratigraphic parameters associated with the drillings (elevation and lithotechnical units) were interpolated using the inverse distance weighting technique, employing 4 neighbouring points and an exponent of 2, for generating a voxel-based solid model (Liu et al. 2021). A high-fidelity filter was adopted to honour the value of the control point variable (Ciampi et al. 2022). The domain of the data-driven block model consists of a 3D mesh with a node resolution of 10 m (x) × 10 m (y) × 0.2 m (z). The model features 153 × 123 × 106 voxels in three dimensions and spans from -66 to 144 m a.s.l., covering an area of about 130 ha. A 4D modelling, performed based on the temporal evolution of coastal deposits inferred from 1960 and 2020 aerial photos, provides a volumetric assessment of geomorphological processes and erosional dynamics over time. The resulting digital models paint data-driven 3D geologic structures and capture lateral-vertical variations of lithotechnical units, employing a vertical exaggeration factor of 1.5 to highlight lithologic transitions (Fig. 9).

The 3D geological model reproduces the subsurface geological architecture as well as the spatial relationships between the various geological units. In contrast to conventional 2D representation techniques, which omit significant portions of the spatial domain, the 3D model empowers anatomical restitution of entire subsurface volumes through solid reconstruction, paving an opportunity for overall interpretation and qualitative/quantitative analysis of the geological bodies' spatiotemporal distribution (Royer et al. 2015; Antonielli et al. 2023). A volumetric computation in post-processing operations reveals the deposition of about 0.8 million m^3 of filling material in the last 60 years, testifying to advancing littoral dynamics driven by an increased anthropic presence along the coast over time (Ouillon 2018). Besides, dynamic extraction of 2D engineering geological cross-sections from the data-driven solid model encourages numerical modelling of the local seismic response (Fig. 10).

4.5 Numerical modelling of the local seismic response

To evaluate the seismic response of the studied area, a subsequent phase of numerical modelling was conducted using the LSR 2D software (STACEC s.r.l.). This tool enables two-dimensional modelling of seismic motion propagation via an equivalent linear analysis, applying finite element methods in the time domain under total stress conditions and incorporating a viscoelastic rheological behaviour based on the

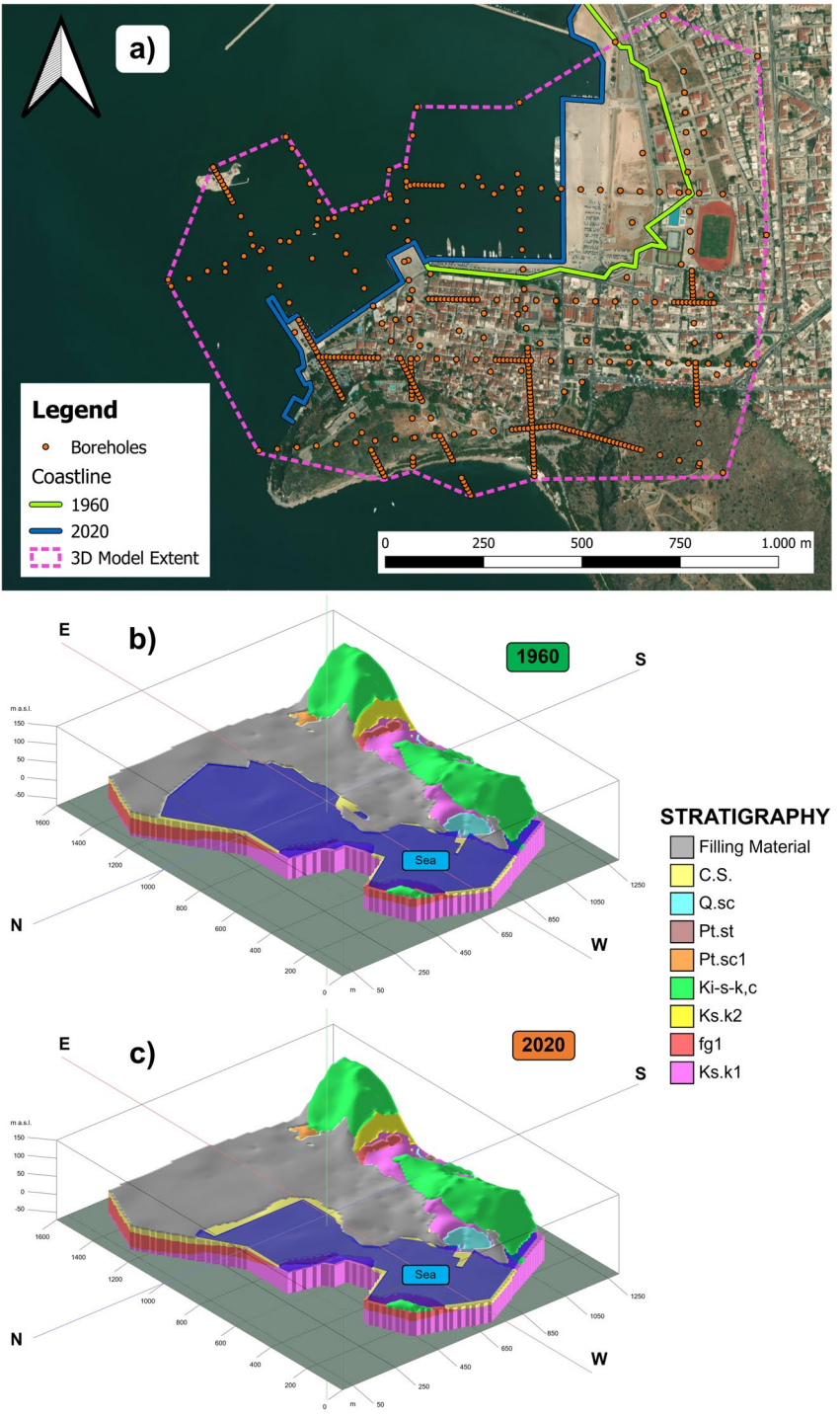

Fig. 9 Location of boreholes in the model domain extent and mapping of the 1960 and 2020 coastline (**a**). Multi-temporal and 3D geological engineering model for 1960 (**b**) and 2020 (**c**)

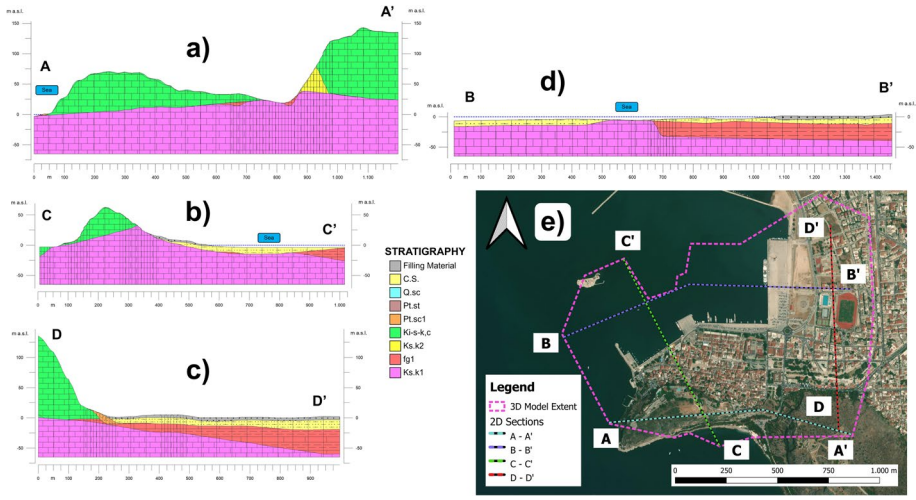

Fig. 10 Examples of 2D geological cross-sections extrapolated from the 3D engineering geological model (**a**, **b**, **c**, **d**) at mapped lines (**e**)

Kelvin–Voigt model. Physical, geophysical, and decay parameters (such as shear stiffness and damping degradation curves), designated to the geological-technical units (refer to Table 1), were assigned to the multilayer structure, and the preselected seismic inputs were applied to the infinite half-space representing the seismic bedrock. Additionally, the model was discretised into triangular meshes with an approximately 2 m resolution grid. This grid was automatically generated by the software to achieve optimal resolution, considering the varying S-wave velocities of the layers and a maximum analysis frequency of 20 Hz. Free-field conditions (i.e., damping in the X and Z directions) were applied on the lateral borders, with a kinematic constraint on vertical motion at the base of the domain within the infinite half-space. Numerical simulations were conducted for all reconstructed engineering geological cross-sections using one of the extracted set of 7 time histories. According to ICMS (2008) guidelines, these time histories were selected for the number of inputs required for numerical simulations, with 50, 475, and 2000-year return periods. The ESM database and the Rexel software were used, with a spectrum-compatibility period range of 0.15–2 s and tolerances of 10% lower and 30% upper.

This numerical analysis made it possible to determine, for each control point along the cross-sections (indicated by red dots in Fig. 11) and for each analysed return period, the following informations: the Fourier amplitude spectrum, the amplification factor (AF) according to ICMS (2008) standards, and the elastic response spectrum (with 5% damping).

The results from the 2D modelling, expressed as horizontal acceleration, indicate higher values in the soft soils along the valley edge, likely due to diffraction and reflection of seismic waves caused by a non-horizontal, shallow bedrock. An incremental rise in acceleration was observed at the top of elevations, such as Acronafplia Hill. This increase can be attributed to the ridge effect, where the focusing of seismic waves leads to amplification at the peak of the ridge.

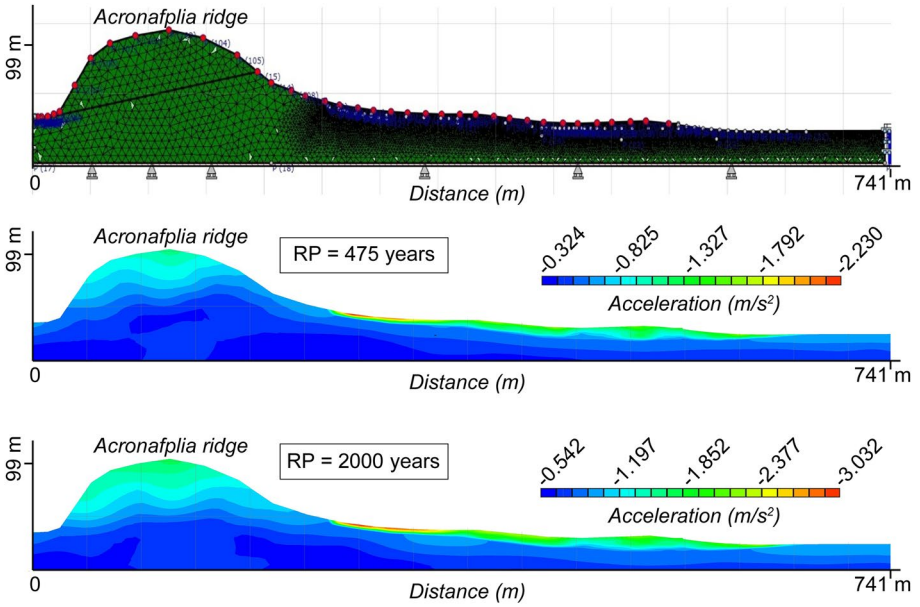

Fig. 11 Results of the 2D numerical modelling along Sect. 2 of Fig. 2: the maximum horizontal acceleration in the subsoil, modelled for the return period (RP) of 475 and 2000 years, is plotted by the software LSR 2D; red dots correspond to the control points where the results were saved. Higher acceleration values are found at the top of the Acronafplia ridge and in the coastal plain, where site amplification effects are expected (modified after Antonielli et al. 2022)

4.6 Local seismic response from recorded earthquakes

For the present study, a temporary seismic net of 4 seismic stations (Fig. 7) instrumented by 3-component velocimeters (2.0 Hz eigenfrequency) by SARA Electronics Instruments was also installed in a continuous acquisition mode, distributed in peculiar places of the Nafplio town which have been selected based on the results derived from HVNR analysis (see Sect. 4.2). The temporary seismic net allowed recording earthquakes from far to very far field conditions that have been used to compute instrumental amplification functions, adopting the Spectral Standard Ratios (SSR) approach by Borcherdt (1970) as well as the Horizontal-to-Vertical Earthquake Spectral Ratio (HVER). The seismic net was operative from 17 to 25 September 2022 and recorded more than 50 weak motions ($1 < M < 5$), which were also recorded by the Hellenic Seismic Network (https://bbnet.gein.noa.gr/).

Among the total recorded earthquakes, 42 signals only were considered suitable to be processed and were divided into two different clusters magnitude-distance (from Nafplio) (Fig. 12): cluster 1, $1 < M < 2.5$ (19) until 150 km with main sources W-NW (Table 3) and cluster 2, $2.6 < M < 5$ (23) until 500 km with main sources W and S (Table 4); for each cluster the following elaborations were firstly performed:

- Trim of the continuous records using the onset time of events.
- Fast Fourier Transform (FFT) calculation for each component of all the selected earthquakes;

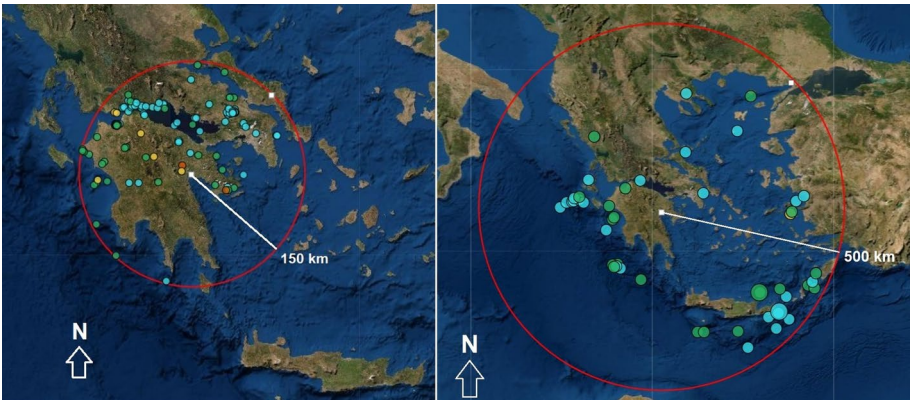

Fig. 12 Localisation of the earthquakes around Nafplio town for the two clusters considered in the period 17–25 September 2022: Cluster 1, $1 < M < 2.5$ until 150 km far (left) and Cluster 2, $2.6 < M < 5$ until 500 km far (right)

Table 3 Earthquake selected for cluster 1, $1 < M < 2.5$ up to 150 km with main sources W-NW (where Ml is the Richter Magnitude)

Date	Time (UTC)	Lat	Long	Depth (Km)	Ml
17/09/2022	12:50:51	38.166	21.6463	19.2	2.1
17/09/2022	17:51:55	36.9699	21.351	15.9	2.5
19/09/2022	8:58:33	37.3755	23.2983	79.4	2.1
20/09/2022	9:35:43	37.4725	22.2821	16	1.7
20/09/2022	11:12:59	38.3043	23.3153	7.8	2
20/09/2022	11:50:45	37.6204	23.2512	15.5	2
20/09/2022	17:58:29	37.3801	23.3395	22.1	1.7
20/09/2022	21:39:56	37.6749	22.6474	63.6	1.7
20/09/2022	23:12:45	38.1715	21.6463	20	2
21/09/2022	0:47:15	37.4162	23.3208	14.9	1.5
21/09/2022	4:37:16	37.4382	23.1404	16.1	1.6
21/09/2022	7:10:34	37.408	23.4206	19.1	1.6
21/09/2022	14:02:18	37.462	21.9868	10.4	2.5
24/09/2022	5:28:00	37.9555	22.5893	10.3	1.3
24/09/2022	6:08:19	37.9697	22.5851	10.9	1.5
24/09/2022	9:28:37	37.8223	22.7637	7.4	1.4
24/09/2022	19:59:39	37.5577	23.5703	11.2	1.3
25/09/2022	3:05:57	38.237	22.8543	12.8	1.1
25/09/2022	6:38:07	37.9628	22.5993	13.7	2.3

- Application of the smoothing function by Konno and Ohmachi (1998) on the FFT spectra (considering one single window for each earthquake);
- Computation of the HVER function as the ratio between the quadratic mean of the two horizontal (H) FFT spectra and the vertical (V) FFT spectrum for each selected earthquake;

Table 4 Earthquakes selected for cluster 2, 2.6 < M < 5 until 500 km with main sources W and S (with Ml equal to Richter Magnitude)

Date	Time (UTC)	Lat	Long	Depth (Km)	Ml
17/09/2022	18:41:41	35.5728	25.8261	15.7	4.2
18/09/2022	1:49:07	35.554	25.8073	18.9	2.7
18/09/2022	14:45:29	38.156	21.6591	26.7	2.8
19/09/2022	3:31:37	35.0775	26.424	10.4	4.2
19/09/2022	10:17:38	37.9399	20.2263	17.5	2.8
19/09/2022	11:40:35	37.9065	20.0867	9.4	2.7
19/09/2022	22:43:20	37.8085	20.3641	6.8	3.1
20/09/2022	1:31:27	39.4048	20.7069	15.7	2.9
20/09/2022	7:02:02	37.8745	20.2469	10.7	2.6
20/09/2022	11:53:50	35.5733	25.8257	18.2	3.4
20/09/2022	16:42:40	37.131	21.0818	5.8	3.2
21/09/2022	6:27:04	37.9166	20.159	26.4	2.8
21/09/2022	9:59:58	38.3418	22.1169	11.4	2.7
21/09/2022	17:33:31	39.0202	23.5368	11.8	2.9
23/09/2022	0:00:03	37.847	20.0583	10.9	2.8
23/09/2022	3:43:14	36.2256	21.3721	13.2	2.7
23/09/2022	7:30:11	36.2622	21.2622	23.5	2.8
23/09/2022	14:15:52	35.6708	27.5226	25.7	3.9
23/09/2022	22:20:38	34.8898	26.7325	6.5	3.4
24/09/2022	13:21:46	36.2732	21.427	16.9	2.6
24/09/2022	15:41:34	36.2494	21.3959	14.3	2.6
24/09/2022	18:16:20	36.2439	21.4197	28.8	3.2
25/09/2022	2:04:08	39.537	25.145	13.7	2.6

- Computation of the mean HVER function, with associated standard deviation, for each site by averaging the HVER calculated for all the earthquakes in the cluster (Fig. 13).

5 Discussion

By comparing HVNR and HVER for the 4 sites distributed in Nafplio town, it has been confirmed that the absence of amplification effects results in the case of outcropping bedrock, i.e., for SS1 (A in Fig. 13) situated close to the town centre; for the SS2 (B in Fig. 13) station, the HVER analysis reveals weak amplification effects at frequencies lower than 2 Hz, probably related to the location of the station at the top of a ridge. Moreover, in the case of sites SS3 (C in Fig. 13) and SS4, localised downtown, HVNR and HVER are in good agreement and confirm evidence of amplification effects at resonance frequencies of about 2.5 Hz for SS3 (C in Fig. 13) and 7 Hz for SS4 (D in Fig. 13). The locations of the temporary earthquake recording stations (SS*n#*) are visible on Fig. 7. These results highlight the different local geological conditions of the subsoil and the deepening of the seismic bedrock moving towards the northern sector of the town.

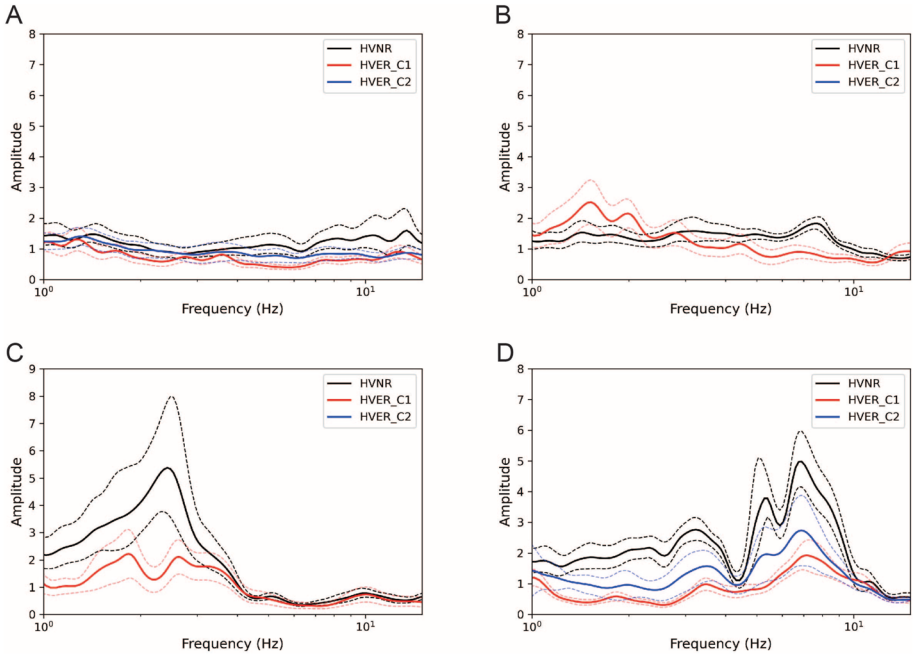

Fig. 13 Horizontal-to-vertical spectral ratio from seismic ambient noise (HVNR) and earthquakes (HVER); red solid lines are referred to the earthquakes belonging to Cluster 1 of Fig. 12 and blue solid lines are referred to the earthquakes belonging to Cluster 2 of Fig. 12: **A** SS1; **B** SS2; **C** SS3; **D** SS4 (where SS means Seismic temporary Station number #; the locations of these stations are visible in Fig. 7). Solid and dotted lines in the figures stand for the average curve and upper and lower limits of standard deviation, respectively

Based on the HVER analysis, the SS1 station was chosen as the reference site, and to better constrain the local seismic response analysis, the selected earthquake signals were used to define the amplification functions by computing the standard spectral ratio (SSR—Borcherdt 1970) according to the following steps:

- standard spectral ratios SSR were computed for each measurement site as the ratio between homologous components (E-W and N-S) of the earthquake recorded in SS2, SS3, SS4 and in the reference site SS1;
- the mean SSR function was computed, with associated upper and lower standard deviation limits, for each measurement site by averaging the SSR calculated for all earthquakes of the cluster (Fig. 14).

Results from SSR analysis were compared with the outputs from 1 and 2D numerical modelling under elastic conditions to validate the amplification effects observed in Nafplio town. In general, it is worth observing (Fig. 14):

- A good agreement in the main amplification frequencies at all measurement sites has been obtained except for SS3, Cluster 2 (D), due to recording fails;
- Amplification amplitudes from SSR functions are generally higher than those from the simulated functions;

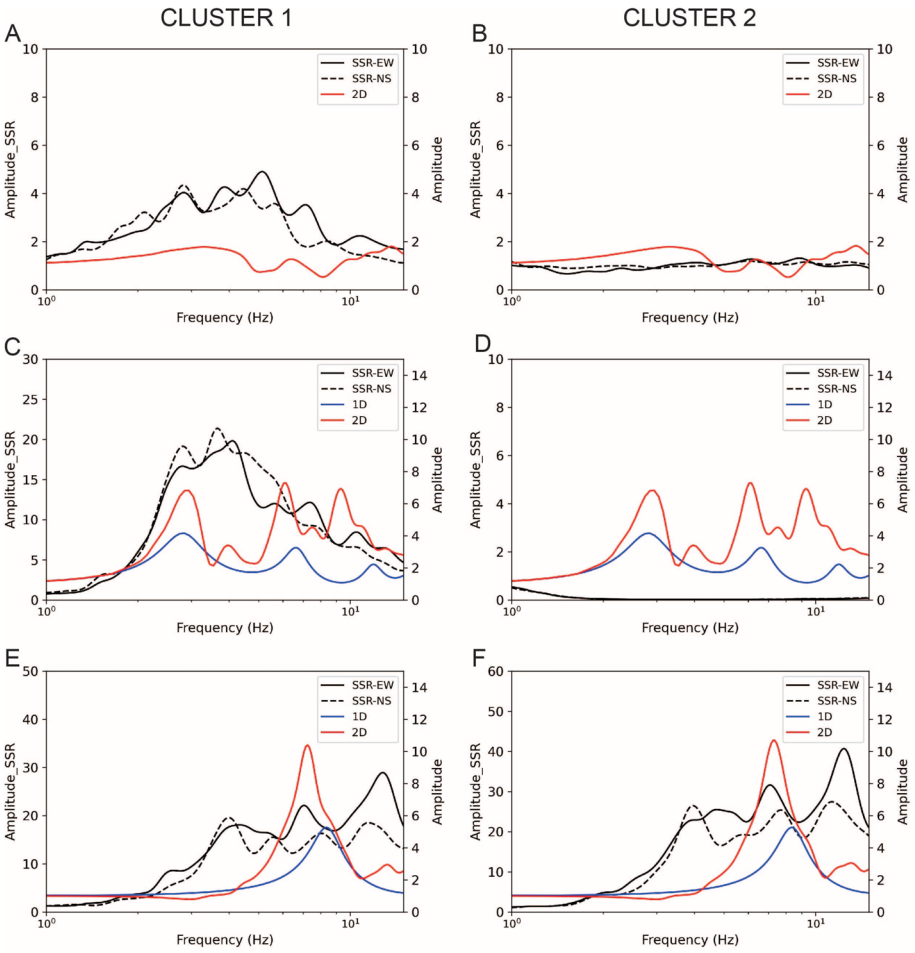

Fig. 14 1D and 2D modelled (elastic conditions) results along with SSR (solid lines east–west and dotted lines mark the north–south components): **A** SS2; **B** SS2, **C** SS3 **D** SS3, **E** SS4 and **F** SS4; (for SS2 site (A and B) was not possible 1D modelling for only outcropping seismic bedrock presence). The two columns refer to earthquake clusters of Fig. 12: Cluster 1, $1 < M < 2.5$ until 150 km far (left) and Cluster 2, $2.6 < M < 5$ until 500 km far

- For the SS4 measurement site, the SSR functions also show amplification frequencies different from the main mode, not evidenced by the outputs of 1D and 2D numerical modelling, probably due to minor seismic impedance contrasts related to the local soft soil multilayer.

Based on the results obtained from all integrated analyses of the local seismic response to better define and summarise the seismic amplification in the Nafplio studied area, an Amplification Index (AI) was defined as the ratio between output and input integral Fourier amplitude spectra. AI was computed from the modelling results obtained for the 475-years return period in the three frequency ranges associated with the site resonance frequency values observed by the previous analyses (HVNR, HVER, SSR

and numerical modelling), i.e., 1–3, 3–5, and 5–10 Hz. By analysing the values trend of AI along the modelled cross-sections and the corresponding engineering geological model of the subsoil, different zones with a specific seismic response were delimited (Fig. 15). The same procedure has been adopted in all the cross-sections to figure out a map with a zoning of homogeneous seismic response areas (Fig. 16).

As it result of the mapping, 6 zones (in the following NAF-Z#) with typical seismic responses were recognised (Fig. 16):

- NAF-Z1: composed of thick deposits (> 20 m), with resonance frequencies ranging from 1 up to 3 Hz, responsible for a stratigraphic amplification. It is located in the north-eastern part of the historic centre of Nafplio (i.e., SS3 station) and in the northern part of the most recent urbanised area;
- NAF-Z2: consisting of sedimentary deposits with a moderate thickness (between 10 and 20 m), site frequency ranging from 3 up to 5 Hz, and relative amplification

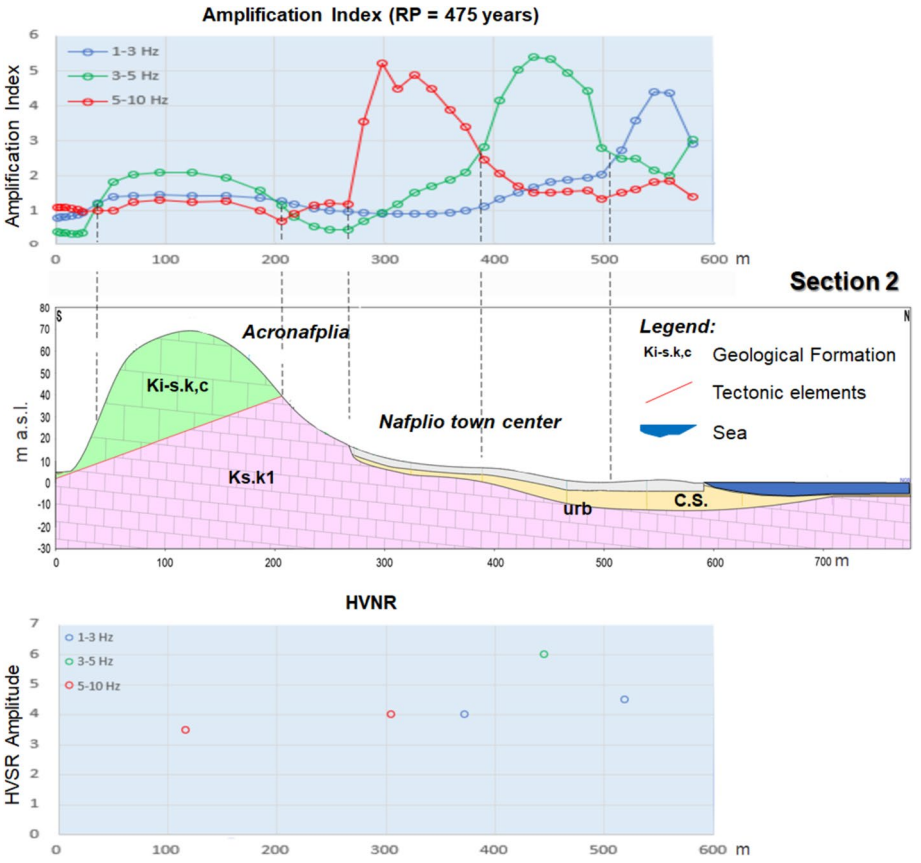

Fig. 15 Example of amplification index (AI) calculated along the cross-Sect. 2 (location in Fig. 2) for 3 period ranges for a 475-years return period (top) according to the resonance frequencies derived from HVNR measurements (bottom). The AI value distribution allowed the contouring of the seismic micro-zones along the modelled cross-section

Fig. 16 Seismic response zonation of the Nafplio study area based on the numerical modelling results. The zoning boundaries follow the study area considered

mainly attributable to a stratigraphic effect. It extends along a strip that crosses the town of Nafplio from east to west, at the south of zone NAF-Z1;

- NAF-Z3: thin deposits (< 10 m) located at the bottom of the carbonate ridges of Palamidi and Acronafplia and in saddle-area which connects the two ridges. The area is characterised by resonance peaks at high-frequency values, ranging from 5 up to 13 Hz (i.e., SS4 station); the amplifying phenomenon is connected both to a stratigraphic effect (main peak at 5 Hz about) and probably to valley edge effects, as better identified consistently by SSR functions and secondarily 2D modelling (i.e. 13 Hz about);
- NAF-Z4: area mostly represented by soft soil deposits, characterised by the absence of amplification and, in some cases, by seismic deamplification; this zone is extended along a narrow strip that extends along the Arvanitia route, south of the Acronafplia ridge, up to the north-west of the aforementioned relief;
- NAF-Z5: includes a wide portion of the rocky ridge of Acronafplia, and it is characterised by a weak amplification, probably linked to topographical effects, with frequencies of interest ranging from 3 up to 5 Hz like showed especially from SSR functions (i.e., SS2 station);
- NAF-Z6: corresponds to the northern slope of the Palamidi hill, and it is characterised by seismic deamplification or absence of amplification.

Elastic (5% damping) response spectra were also derived for each homogeneous seismic zone for the three considered return periods (i.e., 50, 475, and 2000 years) by averaging the elastic response spectra of seven control points included in each zone. Figure 17 shows the response spectra for the 475-years return period obtained by the LSR study for each zone

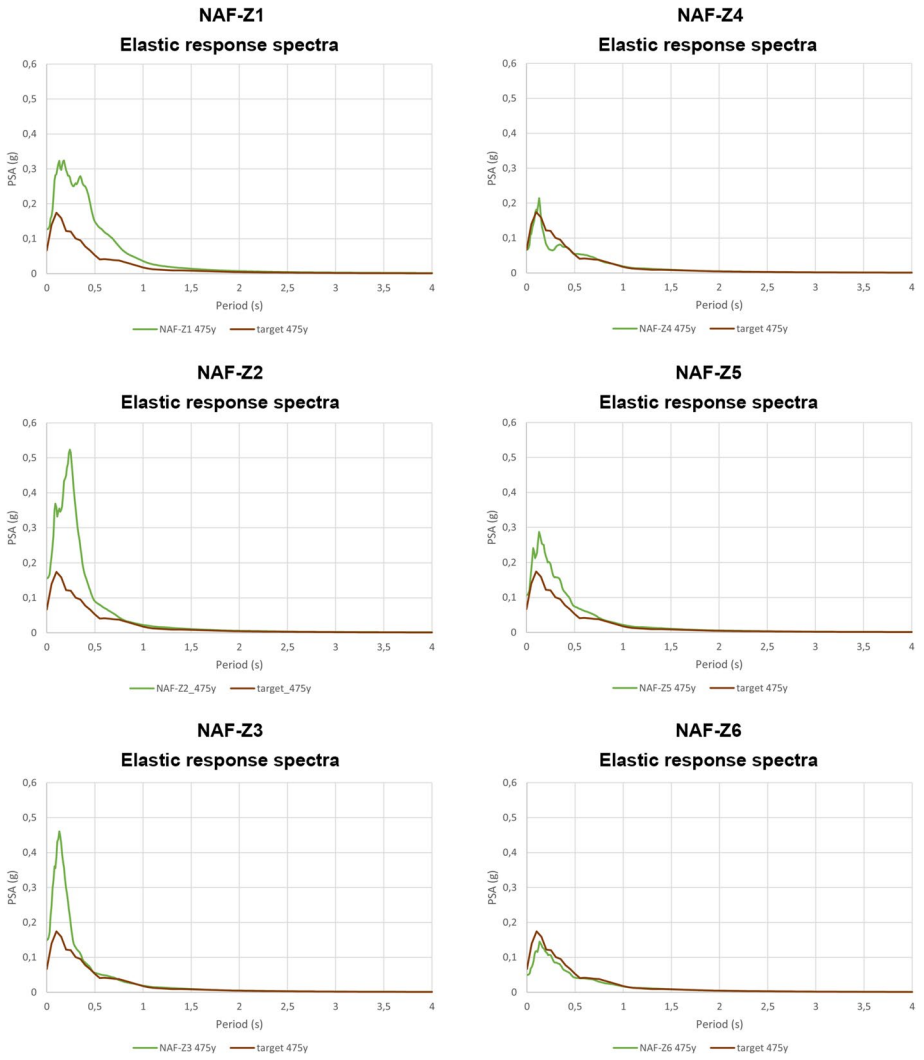

Fig. 17 Elastic response spectra (5% damping) for the return period of 475 years obtained at Nafplio for the 6 zones identified by numerical modelling; the target elastic response spectra obtained according to the basic seismic hazard analysis are also shown

compared with the target response spectra obtained for the 475-years return period by the basic seismic hazard analysis.

Except for NAF-Z6 located on the Palamidi ridge, which presents response spectra lower than the targets, all the obtained response spectra show a significant amplification for all period ranges with respect to the input spectra representative of basic seismic hazard obtained at the seismic bedrock (cf. 3.2 paragraph). In particular, NAF-Z2 e NAF-Z3 show the maximum seismic amplification, especially in the period band between 0.1 and 0.4 s, while NAF-Z1 is characterised by a lower amplification for a larger period band (0.1–0.7 s); NAF-Z4, at the bottom of the Acronafplia ridge, reveals a quite negligible

seismic amplification. It is worth noting that also NAF-Z5, located on the Acronafplia ridge, is characterised by clear amplification, especially in the period range 0.1–0.5 s; this evidence can be referred to topographic amplification effects, not initially detected by seismic ambient noise measurements (Figs. 7 and 8) but evidenced as by HVER, SSR functions and 2D numerical modelling.

6 Conclusion

Over the last decades, the protection and preservation of historical and cultural heritage with respect to seismic hazard-related damages have become increasingly important for national and local authorities. In the framework of the European project STABLE (H2020 RISE-Marie Curie Action), this study was carried out to evaluate seismic site effects in the Nafplio town area, an important historical centre located in the northeastern Peloponnese, Greece, where a complex geological setting and a medium-to-high regional seismic hazard converge.

To assess the local seismic response, a comprehensive approach was adopted. This includes the reconstruction of the subsoil's engineering geological profiles based on field surveys and previous site investigations, a seismic hazard study, and geophysical investigations utilising seismic ambient noise measurements. A 3D geological model of the subsoil was developed, and 2D numerical modelling was performed along selected cross-sections to carry out a detailed seismic microzonation of the area.

Results by seismic ambient noise analysis revealed that significant seismic resonance exists in the different zones of Nafplio. In particular, the HVNR and HVER functions obtained from the seismic ambient noise measurements and earthquake measurements carried out on the recent deposits of the Nafplio coastal plain, respectively, are characterised by a marked peak having frequency values of 2–5 Hz in the historical town centre and 1–2 Hz in the modern town area. These findings were further confirmed by 1D and 2D numerical models, which highlighted amplification phenomena with high horizontal acceleration values across all considered return periods (50, 475, and 2475 years), particularly in the alluvial plain, along ridge slopes, and at the top of the Acronafplia ridge. SSR functions, calculated from earthquake recordings at four seismic stations, corroborated the amplification frequencies identified in the numerical models.

By using the distribution of amplification index (AI) values derived from the numerical modelling across three frequency ranges (i.e., 1–3, 3–5 and 5–10 Hz), different zones were mapped, enveloping areas with expected similar seismic response. In each zone, an elastic response spectrum for the three selected return periods was derived; maximum values in terms of PSA, especially in the period range 0.1–0.5 s were observed. This period range could be significant considering the structural period of the buildings in Nafplio town centre (microzones NAF-Z1 and NAF-Z2).

These results output that a significant seismic amplification characterises the studied area which can be related to a complex geological and geomorphological setting (i.e., including stratigraphic and topographic peculiarities). These findings evidence the relevance of combining and integrating data from accurate field surveys, quick geophysical investigations, acquisition, and analysis of experimental data (earthquakes), as well as numerical modelling to derive response spectra for new buildings design as well as reinforcement interventions of already existing buildings in the framework of seismic risk mitigation strategies.

Acknowledgements The activities of M. Fiorucci and R. Iannucci were mainly performed during their post-doctoral research fellowship at the Department of Earth Sciences of Sapienza University of Rome. We thank the owners of Sokaki Cafe', Kapodistria Hotel, Downtown Hotel and Nafplia Palace Hotel for allowing the installation of the temporary seismic net. We dedicate this paper to the memory of our colleague Dr. Luigi Marino, prematurely passed away, who put his passion and dedication into this work.

Funding This work was supported by H2020-MSCA-RISE-2018 STABLE (STructural stABiLity risk assEssment) Project. The field activities were partially supported by the project "Integration of seismic ambient noise measurements and engineering geological surveys for the purposes of local seismic response study" (prot. n. AR21916B7BB6A787; P.I. R. Iannucci) of 2019 Research Initiation Projects of Sapienza University of Rome.

Declarations

Conflict of interest The authors have no relevant financial or non-financial interests to disclose.

References

Anastasiadis A, Raptakis D, Pitilakis K (2001) Thessaloniki's detailed microzoning: subsurface structure as basis for site response analysis. Pure Appl Geophys 58:2597–2633

Antonielli B, Bozzano F, Fiorucci M et al (2021) Engineering-geological features supporting a seismic-driven multi-hazard scenario in the Lake Campotosto area (L'Aquila, Italy). Geosciences 11(3):107

Antonielli B, Iannucci R, Ciampi P et al (2023) Engineering-geological modeling for supporting local seismic response studies: insights from the 3D model of the subsoil of Rieti (Italy). Bull Eng Geol Environ 82(6):235

Antonielli B, Bozzano F, Ciampi P, Fiorucci M, Iannucci R, Inciocchi D, Karastathis V, Maniatakis C, Martino S, Mouzakiotis A, Rivellino S, Saroglou C, Tsirogianni A, Spyrakos C (2022) Analysis of local seismic response in the historical city centre of Nafplio (Greece). In: proceedings of the third european conference on earthquake engineering and seismology—3ECEES (pp. 4728–4736). Congress

Apostolidis E, Koutsouveli A (2010) Engineering geological mapping in the urban and suburban region of Nafplion city (Argolis, Greece). Bull Geol Soc Greece 43(3):1418–1427

Armijo R, Meyer BGCP, King GCP, Rigo A, Papanastassiou D (1996) Quaternary evolution of the Corinth Rift and its implications for the Late Cenozoic evolution of the Aegean. Geophys J Int 126(1):11–53

Atkinson GM, Boore DM (1995) Ground-motion relations for eastern North America. Bull Seismol Soc Am 85(1):17–30

Aubouin J (1959) Contribution à l'étude géologique de la Grèce septentrionale: les confins de l'Epire et de la Thessalie. Ann Géol Pays Hellén 10:1–403

Aubouin J, Bonneau M, Celet P et al (1970) Contribution à la géologie des Hellénides: le Gavrovo, le Pinde et la zone ophiolitique subpélagonienne. Ann Soc Géol Nord 90:277–306

Aydin ÖL, Karimi B, Kazaz İ (2025) Geotechnical and geophysical investigations on local site effects in Erzurum Türkiye. Nat Hazards. https://doi.org/10.1007/s11069-025-07298-w

Baker JW (2008) An introduction to probabilistic seismic hazard analysis (PSHA). White Pap Version 1.3 1:72

Bala A, Toma-Danila D, Ciugudean-Toma V (2023) 3D geological model and geotechnical data for Bucharest: necessary input for assessing local seismic hazard of a densely populated area. Acta Geod Geophys 58(2):175–196

Beresnev IA, Atkinson GM (1997) Modeling finite-fault radiation from the ω n spectrum. Bull Seismol Soc Am 87(1):67–84
Boore DM (1983) Stochastic simulation of high-frequency ground motions based on seismological models of the radiated spectra. Bull Seismol Soc Am 73(6A):1865–1894
Borcherdt RD (1970) Effects of local geology on ground motion near San Francisco Bay. Bull Seismol Soc Am 60(1):29–61
Bortolotti V, Carras N, Chiari M, Fazzuoli M, Marcucci M, Photiades A, Principi G (2003) The Argolis Peninsula in the palaeogeographic and geodynamic frame of the Hellenides. Ofioliti 28(2):79–94
Bortolotti V, Chiari M, Marroni M, Pandolfi L, Principi G, Saccani E (2013) Geodynamic evolution of ophiolites from Albania and Greece (Dinaric-Hellenic belt): one, two, or more oceanic basins? Int J Earth Sci 102:783–811
Castellaro S, Mulargia F (2009) The effect of velocity inversions on H/V. Pure Appl Geophys 166(4):567–592
Ciampi P, Esposito C, Bartsch E, Alesi EJ, Petrangeli Papini M (2021) 3D dynamic model empowering the knowledge of the decontamination mechanisms and controlling the complex remediation strategy of a contaminated industrial site. Sci Total Environ 793:148649
Ciampi P, Esposito C, Cassiani G et al (2022) Contamination presence and dynamics at a polluted site: spatial analysis of integrated data and joint conceptual modeling approach. J Contam Hydrol 248:104026
Cornell CA, Vanmarcke EH (1969) The major influences on seismic risk. In: proceedings of the fourth world conference on earthquake engineerin. vol. 1, pp. 69–83
Danciu L, Tselentis GA (2007) Engineering ground-motion parameters attenuation relationships for Greece. Bull Seismol Soc Am 97(1B):162–183
Ferentinos G, Papatheodorou G, Collins MB (1988) Sediment transport processes on an active submarine fault escarpment: Gulf of Corinth, Greece. Mar Geol 83(1–4):43–61
Fotiadis Mitropoulos D (2006) Geologic Map 1:5.000 region of ''Nafplion'', Ed. HSGME
Gaudiosi I, Del Monaco F, Milana G, Tallini M (2014) Site effects in the Aterno River Valley (L'Aquila, Italy): comparison between empirical and 2D numerical modeling starting from April 6th 2009 Mw 6.3 earthquake. Bull Earthq Eng 12:697–716
Georgiou C, Galanakis D (2010) Neotectonic study of urban and suburban Nafplio area (Argolida-Greece). Bull Geol Soc Greece XLIII(3):1428–1437
Giallini S, Sirianni P, Pagliaroli A et al (2024) Reconstruction of a subsoil model for local seismic response evaluation through experimental and numerical methods: the case of the Wellington CBD, New Zealand. Eng Geol 330:107413
Haghshenas E, Bard PY, Theodulidis N (2008) Empirical evaluation of microtremor H/V spectral ratio. Bull Earthq Eng 6(1):75–108
Hakimov F, Domej G, Ischuk A, Reicherter K, Cauchie L, Havenith HB (2021) Site amplification analysis of dushanbe city area, tajikistan to support seismic microzonation. Geosciences 11(4):154
Hakimov F, Havenith HB, Ischuk A, Reicherter K (2024) Assessment of site effects and numerical modeling of seismic ground motion to support seismic microzonation of Dushanbe City, Tajikistan. Geosciences (Basel) 14(5):117
Iannucci R, Antonielli B, Coradini M et al (2022) Analysis of the local seismic response in the Strovolos Municipality (Nicosia District, Cyprus). Ital J Eng Geol Environ 1:43–53
ICMS Working Group (2008) Indirizzi e criteri per la microzonazione sismica—guidelines for seismic microzonation. Conferenza delle regioni e delle province autonome. Dipartimento della Protezione Civile. https://www.centromicrozonazionesismica.it/it/download/category/3-linee-guida
Karakaisis GF, Papazachos CB, Scordilis EM (2010) Seismic sources and main seismic faults in the Aegean and surrounding area. Bull Geol Soc Greece 43(4):2026–2042
Karastathis VK, Karmis P, Novikova T et al (2010) The contribution of geophysical techniques to site characterisation and liquefaction risk assessment: case study of Nafplion City, Greece. J Appl Geophys 72(3):194–211
Kham M, Semblat JF, Bouden-Romdhane N (2013) Amplification of seismic ground motion in the Tunis basin: numerical BEM simulations vs experimental evidences. Eng Geol 155:80–86
Klimis NS, Margaris BN, Koliopoulos PK (1999) Site-dependent amplification functions and response spectra in Greece. J Earthq Eng 3(02):237–270
Konno K, Ohmachi T (1998) Ground-motion characteristics estimated from spectral ratio between horizontal and vertical components of microtremor. Bull Seismol Soc Am 88:228–241
Kottke AR, Rathje EM (2008) Technical Manual for Strata. PEER report 2008/10, Pacific Earthquake Engineering Research Center College of Engineering, University of California, Berkeley (CA)
Liu Z, Zhang Z, Zhou C, Ming W, Du Z (2021) An adaptive inverse-distance weighting interpolation method considering spatial differentiation in 3D geological modeling. Geosciences 11(2):51

Lo Presti D, Luzi L, Pergalani F, Petrini V, Puci I, Signanini P (2002) Determinazione della risposta sismica dei terreni a Castelnuovo Garfagnana (Lucca). Ital Geotech J XXXVI:3
Macerola L, Tallini M, Di Giulio G, Nocentini M, Milana G (2019) The 1-D and 2-D seismic modeling of deep quaternary basin (Downtown L'Aquila, Central Italy). Earthq Spectra 35(4):1689–1710
Makropoulos K, Kaviris G, Kouskouna V (2012) An updated and extended earthquake catalogue for Greece and adjacent areas since 1900. Nat Hazards Earth Syst Sci 12(5):1425–1430
Martino S (2024) Evidence of unstable rock cliffs from vibrational behavior: challenges in coupling engineering-geological and geophysical approaches. Ital J Eng Geol Environ 2:S-05
Martino S, Lenti L, Gélis C et al (2015) Influence of lateral heterogeneities on strong-motion shear strains: simulations in the historical Center of Rome (Italy). Bull Seismol Soc Am 105(5):2604–2624
Martino S, Caprari P, Della Seta M et al (2020) Influence of geological complexities on local seismic response in the municipality of Forio (Ischia island, Italy). Ital J Eng Geol Environ 2:O-04
McGuire R (1993) The practice of earthquake hazard assessment. International Association of seismology and physics of the earth's interior and European Seismological Commission.
Mitropoulos D, Zananiri I (2010) Upper quaternary evolution of the northern Argolis Gulf, Nafplio area. Hydrogeological implication. Bull Geol Soc Greece 5(3):1474–1485
Moscatelli M, Albarello D, Scarascia Mugnozza G, Dolce M (2020) The Italian approach to seismic microzonation. Bull Earthq Eng 18(12):5425–5440
Moscatelli M, Vignaroli G, Pagliaroli A et al (2021) Physical stratigraphy and geotechnical properties controlling the local seismic response in explosive volcanic settings: the Stracciacappa maar (central Italy). Bull Eng Geol Environ 80(1):179–199
Motazedian D, Atkinson GM (2005) Stochastic finite-fault modeling based on a dynamic corner frequency. Bull Seismol Soc Am 95(3):995–1010
Noller JS, Wells L, Reinhardt E, Rothaus RM (1997) Subsidence of the harbor at Kenchreai, Saronic Gulf, Greece, during the earthquakes of AD 400 and AD 1928. Eos 78(46):636
Ouillon S (2018) Why and how do we study sediment transport? Focus on coastal zones and ongoing methods. Water 10:390
Papazachos B, Papazachou C (2003) The earthquakes of Greece. Ed Ziti, Thessaloniki
Pergalani F, Pagliaroli A, Bourdeau C et al (2020) Seismic microzoning map: approaches, results and applications after the 2016–2017 Central Italy seismic sequence. Bull Earthq Eng 18:5595–5629
Photiades A (2010) Geological contribution to the tectono-stratigraphy of the Nafplion area (NW Argolis. Greece). Bull Geol Soc Greece 43(3):1495–1507
Polatidis A, Kiratzi A, Hatzidimitriou P, Margaris B (2003) Attenuation of shear-waves in the back-arc region of the Hellenic arc for frequencies from 0.6 to 16 Hz. Tectonophysics 367(1–2):29–40
Reiter L (1990) Earthquake hazard analysis: issues and insights. Columbia University Press
Royer JJ, Mejia P, Caumon G, Collon P (2015) 3D and 4D Geomodeling applied to mineral resources exploration—an introduction. In: Weihed, P. (eds) 3D, 4D and predictive modeling of major mineral belts in Europe. Mineral Resource Reviews. Springer, Cham
Salameh C, Bard PY, Guillier B, Harb J, Cornou C, Gérard J, Almakari M (2017) Using ambient vibration measurements for risk assessment at an urban scale: from numerical proof of concept to Beirut case study (Lebanon). Earth Planets Space 69:1–17
Saroglou C, Bozzano F, Martino S et al (2021) Profiling of the recent deposits of Nafplio coastal plain (Greece) from engineering geological modeling and geophysical surveys. In: proceedings ff 3rd European regional conference of IAEG, Athens, pp. 131–138
Semblat JF, Duval AM, Dangla P (2000) Numerical analysis of seismic wave amplification in Nice (France) and comparisons with experiments. Soil Dyn Earthq Eng 19(5):347–362
Serpetti M, Carlucci R, Di Iorio A et al (2020) Stable: structural stability risk assessment. In: eighth international conference on remote sensing and geoinformation of the environment (RSCy2020), vol. 11524, pp 120–128
Servizio Sismico Nazionale Italiano (2003) Microzonazione sismica di S. Giuliano di Puglia
Sextos A, De Risi R, Pagliaroli A et al (2018) Local site effects and incremental damage of buildings during the 2016 Central Italy earthquake sequence. Earthq Spectra 34(4):1639–1669
Sgobba S, Felicetta C, Russo E et al (2021) The online graphical user interface of REXELweb for the selection of accelerograms from the engineering strong motion database (ESM). In: proceedings of the 39° online GNGTS conference, 22–24 June 2021
Song R, Qin X, Tao Y, Wang X, Yin B, Wang Y, Li W (2019) A semi-automatic method for 3D modeling and visualizing complex geological bodies. Bull Eng Geol Environ 78:1371–1383
Sonmezer YB, Celiker M, Bas S (2019) An investigation on the evaluation of dynamic soil characteristics of the Elazig City through the 1-D equivalent linear site-response analysis. Bull Eng Geol Environ 78:4689–4712

Sornette D, Sornette A (1999) General theory of the modified Gutenberg-Richter law for large seismic moments. Bull Seismol Soc Am 89(4):1121–1130
Sorrentino L, Cattari S, Da Porto F, Magenes G, Penna A (2019) Seismic behaviour of ordinary masonry buildings during the 2016 central Italy earthquakes. Bull Earthq Eng 17(10):5583–5607
Tallini M, Lo Sardo L, Spadi M (2020) Seismic site characterisation of red soil and soil-building resonance effects in L'Aquila downtown (Central Italy). Bull Eng Geol Environ 79:4021–4034
Tunar Özcan N, Ulusay R, Işık NS (2019) Assessment of dynamic site response of the peat deposits at an industrial site (Turkey) and comparison with some seismic design codes. Bull Eng Geol Environ 78:2215–2235
Varone C, Lenti L, Martino S, Semblat JF (2021) Spatial variability of the urban ground motion in a highly heterogeneous site-city configurations. Bull Earthq Eng 19:27–45
Wathelet M, Chatelain JL, Cornou C et al (2020) Geopsy: a user-friendly open-source tool set for ambient vibration processing. Seismol Res Lett 91(3):1878–1889
Wells DL, Coppersmith KJ (1994) New empirical relationships among magnitude, rupture length, rupture width, rupture area, and surface displacement. Bull Seismol Soc Am 84(4):974–1002
Wiemer C, Wyss M (2000) Minimum magnitude of completeness in earthquake catalogs: Examples from Alaska, the western United States, and Japan. Bull Seismol Soc Am 90(4):859–869

Authors and Affiliations

Matteo Fiorucci[1,8] · Salvatore Martino[2] · Benedetta Antonielli[2] · Vasiliki (Betty) Charalampopoulou[3] · Paolo Ciampi[2] · Yawar Hussain[2] · Roberto Iannucci[4] · Daniele Inciocchi[2] · Vassilis Karastathis[5] · Charilaos Maniatakis[6] · Eirini Marinou[3] · Aggelos Mouzakiotis[5] · Stefano Rivellino[2] · Charalampos Saroglou[7] · Athina Tsirogianni[7] · Francesca Bozzano[2]

✉ Salvatore Martino
salvatore.martino@uniroma1.it

[1] Department of Civil and Mechanical Engineering, University of Cassino and Southern Lazio, Via G. Di Biasio 43, 03043 Cassino, FR, Italy

[2] Department of Earth Sciences and CERI Research Centre for Geological Risks, Sapienza University of Rome, P.le Aldo Moro 5, 00185 Rome, Italy

[3] Geosystems Hellas It Kai Efarmoges Geopliroforiakon Systimaton Anonimietaireia, Geosystems Hellas AE (GSH), 225 Imittou Str., 11632 Athens, Greece

[4] ANSFISA National Agency for the Safety of Railways and Road and Motorway Infrastructures, P.le dell'Industria 20, 00144 Rome, Italy

[5] Geodynamic Institute of Athens, Athens, Greece

[6] Department of Structural Engineering, Laboratory for Earthquake Engineering, School of Civil Engineering, National Technical University of Athens, 15780 Zografos, Athens, Greece

[7] Department of Geotechnical Engineering, National Technical University of Athens, 15780 Athens, Greece

[8] European University of Technology , EUt+, European Union, Cassino (FR), Italy